Materials Science & Engineering C 107 (2020) 110342

Contents lists available at ScienceDirect

Materials Science & Engineering C

journal homepage: www.elsevier.com/locate/msec

Additive manufactured porous biomaterials targeting orthopedic implants: A suitable combination of mechanical, physical and topological properties

F. Bartolomeu[a,*], N. Dourado[a], F. Pereira[b], N. Alves[c], G. Miranda[a], F.S. Silva[a]

[a] Center for Micro-Electro Mechanical Systems (CMEMS-UMinho), University of Minho, Campus de Azurém, 4800-058, Guimarães, Portugal
[b] CITAB/UTAD, Departamento de Engenharias, Quinta de Prados, 5001-801, Vila Real, Portugal
[c] Centre for Rapid and Sustainable Product Development Polytechnic Institute of Leiria, Rua General Norton de Matos, Apartado 4133, 2411-901, Leiria, Portugal

ARTICLE INFO

Keywords:
Selective laser melting
Ti6Al4V
Cellular structures
Design tools
Elastic modulus

ABSTRACT

Orthopedic implants are under incessant advancement to improve their interactions with surrounding bone tissue aiming to ensure successful outcomes for patients. A successful biological interaction between implant and surrounding bone depends on the combination of mechanical, physical and topological properties. Hence, Ti6Al4V cellular structures appear as very promising solutions towards the improvement of conventional orthopedic implants. This work addresses a set of fundamental tools that allow improving the design of Ti6Al4V cellular structures produced by Selective Laser Melting (SLM). Three-point bending tests were carried out to estimate the elastic modulus of the produced structures. Morphological analysis allowed to evaluate the dimensional differences that were noticed between the model CAD and the SLM structures. Finite element models (adjusted CAD) were constructed with the experimentally obtained dimensions to replicate the mechanical response of the SLM structures. Linear correlations were systematically found for the dimensions of the SLM structures as a function of the designed model CAD dimensions. This has also been observed for the measured porosities as a function of the designed CAD models. This data can be used in further FE analyses as design guidelines to help engineers fabricating near-net-shape SLM Ti6Al4V cellular structures. Besides, polished and sandblasted surface treatments performed on the Ti6Al4V cellular structures allowed to obtain suitable properties regarding roughness and wettability when compared to as-produced surfaces. The capillarity tests showed that all the analyzed Ti6Al4V structures are able to transport fluid along its structure. The cell viability tests demonstrate Ti6Al4V cellular structures SLM produced did not release toxic substances to the medium, indicating that these structures can assure a suitable environment for cells to proliferate and attach. This study proposes a design methodology for Ti6Al4V cellular structures, that owe suitable mechanical properties but also provide a proper combination of porosity, roughness, wettability, capillarity and cell viability, all of them relevant for orthopedic applications. A Ti6Al4V cellular structured hip implant prototype gathering the suitable features addressed in this study was successfully SLM-produced.

1. Introduction

Selective Laser Melting (SLM) is a high-performance metal additive manufacturing technique that selectively melts a metal powder bed, track by track, and layer by layer to construct a 3D metal part, according to CAD data [1,2]. SLM high design freedom empower an innovative design thinking focused exclusively on the target [3]. By using SLM, engineers can design complex and customized solutions [4,5], such as metallic porous structures, which are almost impossible or unwarrantable to consider when using conventional processing routes such as casting and forging [6].

SLM fabrication of metallic porous materials are in great demand due to these materials potential and benefits that make them extraordinary to apply in biomedical field such as orthopedic implants [7–10]. As an example, Ti6Al4V cellular structures are multifunctional materials capable to address several needs in a single component by tailoring the mechanical, physical and biological properties [4,5]. The accuracy of SLM to fabricate metallic porous materials is an inherent challenge since significant differences are detected when comparing the CAD design with the produced components [11,12]. These dimensional and geometrical differences are systematically detected, as reported by other authors [11,13]. This aspect, empowers the need of predicting these differences and correct the CAD designs accordingly, aiming to obtain porous structures with the desired physical and mechanical

* Corresponding author.
E-mail address: flaviojorgebartolomeu@gmail.com (F. Bartolomeu).

https://doi.org/10.1016/j.msec.2019.110342
Received 2 January 2019; Received in revised form 8 October 2019; Accepted 19 October 2019
Available online 26 October 2019
0928-4931/

properties. Finite element analysis (FEA) [14,15], in parallel with experimental studies, can be used as engineering tool to anticipate and correct SLM production inherent deviations.

A successful biological interaction between implant and bone depends on the combination of mechanical, topological, physical and chemical properties [7,16]. Ti6Al4V have been extensively applied in the orthopedic field owing their high strength-to-weight ratio, good biocompatibility, superior corrosion resistance and lower elastic modulus when compared to stainless steels and cobalt alloys [6,17,18]. However, Ti6Al4V ($\approx$110GPa) has a significant higher elastic modulus when compared to human cortical bone tissue (10–30 GPa) [19–22]. This results in a mismatch stiffness between the implant material and the bone tissue, which leads to a non-adequate stress distribution in the interface [9]. Bone resorption around the implant occurs until a critical moment (usually 10–20 years after total hip arthroplasty surgery) when a revision surgery is needed [23–25]. In this regard, Selective Laser Melting technique is an effective solution to fabricate Ti6Al4V structured materials with an elastic modulus that match with that of bone tissue [9,17,26,27]. These structures can be engineered to reduce the typical over-high stiffness of dense Ti6Al4V implants.

Implant surface topography has a direct effect on the biological response of bone. Several clinical and in vitro studies have demonstrated that moderate surface roughness ($R_a \approx$ 2–4 μm) lead to earlier healing, enhanced cell spreading and tissue integration [28,29]. Also has been reported to enhance the differentiation of osteoblasts cells, to reduce the activity of bone-destroying cells (osteoclasts) as well as to promote a better bone attachment and mineralization [28–31].

Surface energy of an implant is another surface characteristic that plays an important role on implant-bone biological interaction [32]. This characteristic is measured indirectly by the liquid-solid contact angle (wettability), and several studies have found that hydrophilic surfaces tend to enhance cell adhesion, cell differentiation and bone mineralization when compared to hydrophobic surfaces [33–36]. Zhao et al. [33] concluded that osteoblast-cells cultured hydrophilic surfaces produced more differentiation markers represented by increased cell layer alkaline phosphatase specific activity and osteocalcin. The capillarity action is the ability of a fluid to flow into narrow spaces against external forces, such as gravity through cohesive forces [37,38]. Polak et al. [39] and Bai et al. [38] demonstrated that capillary forces play an important role in cells self-seeding and cell attachment on scaffolds surfaces.

In this study Ti6Al4V cellular structures were designed and produced by SLM technique aiming to obtain a proper combination of elastic modulus, porosity, surface roughness and wettability, and also capillarity properties targeting orthopedic implants.

2. Materials and methods

2.1. Material and SLM fabrication details

Ti6Al4V spherical powder (D90 of 40 μm) from *SLM Solutions*® (Germany) was used to produce layer-by-layer the Ti6Al4V cellular structures. Fig. 1 illustrates SLM fabrication route starting with a CAD design modeled in *SolidWorks*, followed by the support's generation using *Materialise Magics*®. Then, *SLM Autofab* was used to perform the numerical slicing. Following the preparation protocol (to achieve suitable temperature and atmosphere), the SLM fabrication layer-by-layer proceeded till the last layer. Afterwards, the Ti6Al4V cellular structures were removed from the platform by cutting the supports and this surface was polished using an abrasive silicon carbide paper (mesh 180). The SLM parameters used in this work were defined through an optimization study regarding the processing parameters for Ti6Al4V, using this SLM equipment [40]. Thus, laser power (90 W), scan speed (600 mm/s), scan spacing (i.e., distance between two consecutive laser scans; 80 μm) and layer thickness (30 μm) were used.

2.2. Selection and design of the cellular structures

When designing cellular structures to integrate in orthopedic implants, several parameters must be considered in order to provide some key properties and in this way improve the osteointegration of the implant. Some of these parameters are the open-cell size, the open-cell morphology, the orientation, the open-cell interconnectivity, the distance between two consecutive open-cells (here called walls) and the ratio surface area to volume. In this study, an admissible design area was considered for the definition of open-cell and wall sizes, which comprehends the following aspects:

(i) Structures with a porosity higher than 50% [13,41] in order to lower the elastic modulus of Ti6Al4V;
(ii) Wall sizes higher than $\approx$100 μm, due to the available laser (having a spot of 89 μm) of the SLM 125HL equipment;
(iii) Open-cell sizes higher than 300 μm and lower than 800 μm, considered optimum for bone ingrowth based on biological studies found in literature [13,41,42].

Table 1 shows the model CAD design details, in which the open-cell and wall sizes, as well as the porosity are presented.

2.3. Morphology and porosity analysis

After removing from the platform, all the structures were prepared to posterior analyses by performing an ultrasonically cleaning during 10 min in other to remove the loose powder. SEM images were obtained for the Ti6Al4V cellular structures, namely isometrically, lateral, top and bottom views (Figs. 4 and 5). SEM images were used to measure the dimensions of the open-cells and walls allowing to estimate the differences between the as-designed (Model CAD) and the produced Ti6Al4V structures. A systematic study was performed in which 60 measurements (20 on each plane for the open-cell and the wall dimensions) were made for SP1, SP2, SP3, SP4 and SP5 structures. The average dimensions of the open-cell and walls for each group were used to create new CADs (here referred as adjusted CADs). These adjusted CADs aim to reproduce the real dimensions measured on the SEM images of the SLM produced specimens.

These structures density was determined by measuring their mass and volume and considering the theoretical density of Ti6Al4V. This density was then used to obtain these structures porosity, considering four specimens for each condition.

2.4. Mechanical testing

Three-point bending flexural tests were conducted in an Instron® 5848 machine. The load signal was obtained with a load cell (2 kN), for an acquisition frequency of 5 Hz. The displacement monitoring was performed using an 8 bit CCD Dolphin camera (Allied Vision Technologies®), with an acquisition frequency of 1.738 fps. At least four different structures were used for each condition. The crosshead displacement rate was set to 0.005 mm/s. Recorded images were post-processed in a home-made MATLAB® routine to monitor a point in the half-span region of the structure. Fig. 2 shows the experimental apparatus used to perform the tests. The apparent elastic modulus was estimated through [43]:

$$E = \frac{K}{48}\frac{L^3}{I} \quad (1)$$

With K standing for the elastic stiffness, L for the loading-span and I for the second moment of area.

2.5. Numerical modelling

Structured finite element meshes were generated for each model

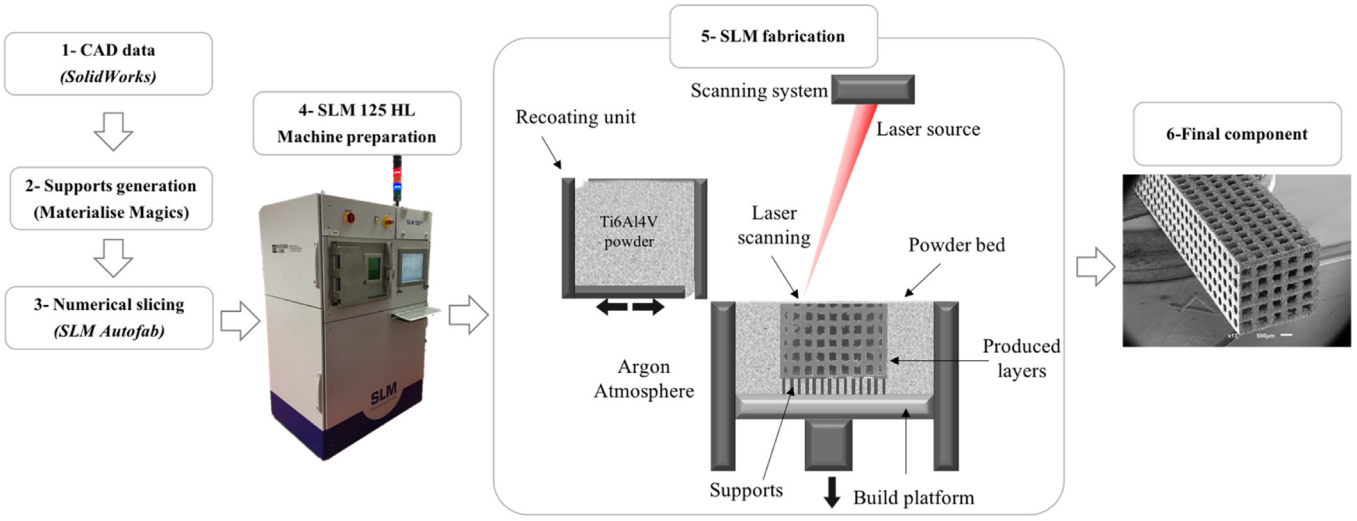

Fig. 1. Schematic representation of SLM technique from CAD to final component.

Table 1
Model CAD design details for the tested specimens.

Structure	Model CAD design details			
	Dimensions (mm^3)	Open-cell size (μm)	Wall size (μm)	Porosity (%)
SP1	4.3 × 4.3 × 56.0	500	300	64.2
SP2	4.8 × 4.8 × 58.5	600	300	70.3
SP3	3.4 × 3.4 × 55.3	500	150	84.0
SP4	3.9 × 3.9 × 56.3	600	150	87.6
SP5	3.6 × 3.6 × 56.0	600	100	93.3

pattern using 20-nodes hexahedral quadratic elements (20-HQE). Fig. 3 shows a typical refined mesh used in the FE analysis and the standardized dimensions (*a* and *b*). Table 2 resumes the dimensions, and with the number nodes, and elements used in the numerical analysis.

Three cylinders were defined with 20-HQE and 15-nodes wedge (triangular prism) element types to simulate the supports and the loading actuator. Contact algorithms were employed to mimic the surface interaction between the specimen and the supports. The bottom supports were impeded to move, while a vertical displacement was ascribed to the top cylinder to apply the load at the mid-span. Elastic properties used in both domains, structures and supports, are presented in Table 3 for Ti6Al4V and steel, respectively.

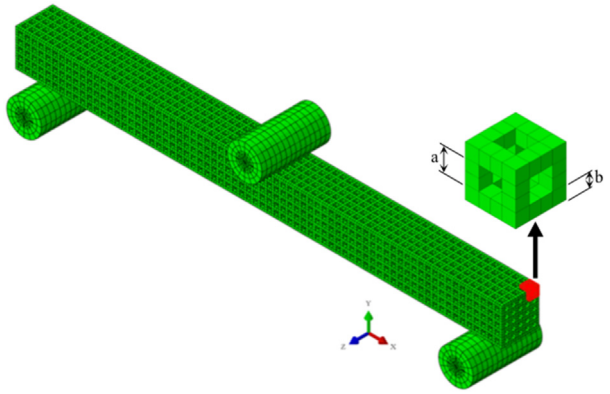

Fig. 3. FE mesh of the SP1 structure.

2.6. Surface preparation and surface roughness measurements

When regarding the surface properties assessments, three types of surfaces were investigated in this study: as-produced, polished and sandblasted. The as-produced surface corresponds to the typical surface obtained after SLM fabrication. The polished surface was obtained using an abrasive silicon carbide paper (mesh 180). The sandblasted surface was prepared using spherical alumina particles (diameter ranging from 106 to 150 μm), blasted during 30 s.

Surface roughness was measured using a surface profilometer

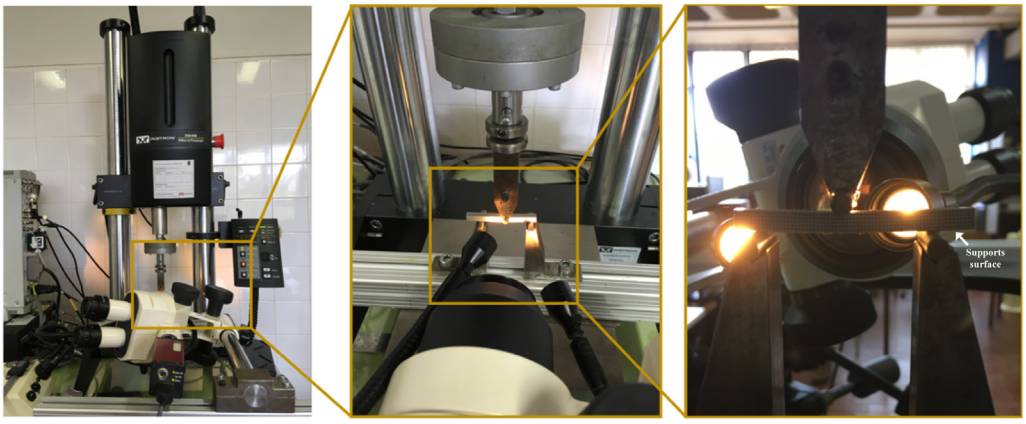

Fig. 2. Mechanical testing system used to perform the three point-bending tests.

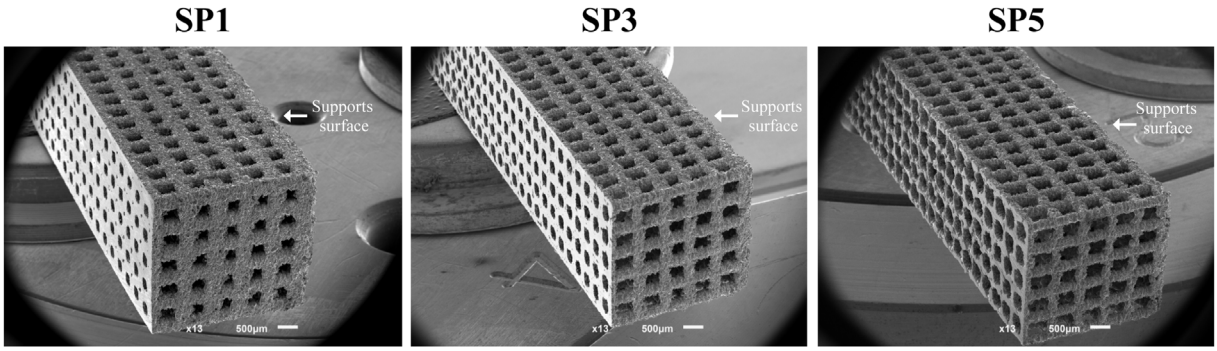

Fig. 4. SEM images of SP1, SP3 and SP5 Ti6Al4V cellular structures.

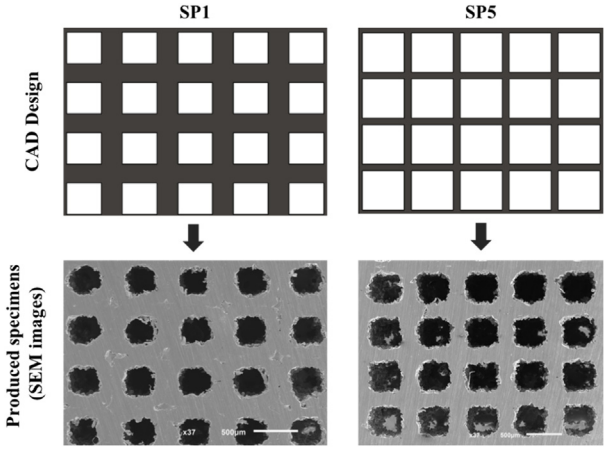

Fig. 5. Comparison between model CAD and the SLM produced structures, at the same scale.

(Surftest SJ 201, Mitutoyo®, Tokyo, Japan). Roughness tests were performed according to ISO 4287-1997 standard, with an evaluation length of 3 mm, a cutoff wavelength of 0.8 mm and a scan speed of 0.25 mm/s. A total of nine measurements were performed for each group using three different structures.

2.7. Wettability and capillarity tests

Contact angle measurements were carried out to determine wettability properties of the Ti6Al4V cellular structures for as-produced, polished and sandblasted surfaces. The measurements were performed on a contact angle system OCA 15 plus (Dataphysics®) using a sessile drop method. For each group, on average, seven droplets of phosphate-buffered saline (PBS) were measured.

Capillarity tests were carried out using a house-made apparatus for video recording. Hence, six time points were defined to quantify the fluid height: 0.0 s (the instant when the specimen touches the fluid), 0.25, 0.5, 0.75, 1.0 and 2.0 s. As-produced specimens from SP1, SP2, SP3, SP4 and SP5 were used to perform these tests. Phosphate-buffered Saline (PBS) fluid was employed to mimic, in some extension, the human body fluids. The fluid heights were measured for all the time points and for all the groups by image analysis.

Table 3
Elastic properties considered for the structures and cylinder domains.

Material	Elastic modulus (GPa)	Poisson's ratio
Ti6Al4V	110	0.30
Steel	210	0.30

2.8. Cell viability

Short-term cytotoxicity tests were carried out on the SLM produced Ti6Al4V cellular structures, following the protocol described by Silva et al. [44,45], in triplicate. The structures were incubated with minimum essential culture medium (MEM) and the medium was extracted and filtered using a 0.45 mm pore-size filter after each time-point (24 h, 7, 14, 21 and 28 days). For all the MEM tests, the material weight-to-extract fluid rate was constant at 0.2 g/ml. Latex extracts with the same extraction protocol were used as positive controls for cell death and culture medium as negative control.

2.9. Statistical analysis

Statistical analyses were carried out using one-way ANOVA with post-hoc Bonferroni multiple comparison test (GraphPad Software, USA), where $p_{value} < 0.05$ was defined as statistical significant, to assess the statistically significant differences of the experimental results (porosity, elastic modulus, surface roughness and live/death cytotoxicity).

Table 2
Resume of FE details.

Structure	Open-cell size *a* (μm)	Wall size *b* (μm)	Number of nodes	Number of elements
SP1 – Model CAD	500.00	300.00	451488	45600
SP1 – Adjusted CAD	387.94	393.38	521424	52668
SP2 – Model CAD	600.00	300.00	503376	50844
SP2 – Adjusted CAD	487.55	393.70	388968	40590
SP3 – Model CAD	500.00	150.00	695136	70224
SP3 – Adjusted CAD	387.65	243.70	645502	65208
SP4 – Model CAD	600.00	150.00	602640	60876
SP4 – Adjusted CAD	493.55	238.69	557520	56316
SP5 – Model CAD	600.00	100.00	485328	49020
SP5 – Adjusted CAD	487.20	194.00	598128	60420

Table 4
Comparison between the model CAD and the produced structures dimensions.

Specimen	Model CAD details			Produced structures measurements		
	Open-cells size (μm)	Walls size (μm)	Porosity (%)	Open-cells size (μm)	Walls size (μm)	Porosity (%)
SP1	500	300	64.2	388 ± 15	393 ± 19	45.0 ± 1.6
	600	300	70.3			
SP2	600	300	70.3	488 ± 13	394 ± 18	54.1 ± 0.8
SP3	500	150	84.0	388 ± 13	244 ± 17	64.0 ± 1.1
SP4	600	150	87.6	493 ± 14	239 ± 14	70.9 ± 0.5
SP5	600	100	93.3	487 ± 9	194 ± 18	78.6 ± 0.9

3. Results and discussion

3.1. Morphological characterization of the SLM structures

Selective Laser Melting technique was used to fabricate five groups of Ti6Al4V cellular structures with different levels of porosity (from 64 to 93%) aiming to reduce the elastic modulus of Ti6Al4Valloy pursuing the use of these structures in orthopedic implants. Fig. 4 shows SEM images of SP1, SP3 and SP5 structures. SP1 and SP5 structures correspond to outmost structures considering the model CAD design porosity. SP1 has the lowest porosity (64.2%), having open-cells of 500 μm, and walls of 300 μm. Contrarily, SP5 has the highest porosity (93.3%) with open-cells of 600 μm and walls of 100 μm.

In order to compare the model CAD design with the SLM produced specimens, a morphological study was conducted using SEM images of all the specimen's group investigated. For that purpose, the open-cell and wall sizes of all of the structures were measured through image analyses. SEM images from the front, the lateral and the top plane were used in these measurements. Fig. 5 shows an illustrative comparison between model CAD design and the SLM produced structures for SP1 and SP5. Table 4 presents the average results (± standard deviation) regarding the open-cell and wall sizes.

Table 4 shows systematic differences between the model CAD and the SLM structures. The five groups investigated exhibit, on average, an open-cell size 111 ± 2 μm lower than the model CAD. Contrarily, the wall size is on average 93 ± 2 μm higher than that defined on the model CAD design. Fig. 5 and Table 4 show that these dimensional deviations were detected for all the specimens investigated (SP1 to SP5). These differences between the model CAD and the SLM specimens are inherent to SLM fabrication as reported in other studies [12,13,46]. In fact, the production of porous structures, with approximately 100 μm smaller open-cells and 100 μm thicker walls can be found in literature [11,13,47]. As an example, Q. Ran et al. [46] designed porous Ti6Al4V specimens having open-cells with 500, 700 and 900 μm of diameter. The produced parts exhibited smaller pore sizes when compared to the CAD design, with open-cells of 400, 600 and 800 μm, respectively. The differences in heat transport between powder and solid material leads to the powder sticking to the solid surface, being pointed as accountable for these deviations [46]. Moreover, some of the powder in the vicinity of the laser melted zones partially melts, thus increasing the dimension of the walls. As a consequence, lower open-cells sizes are obtained, when compared to the CAD design.

Fig. 6 shows the linear correlations between the measured open-cell and the wall sizes, and the corresponding CAD model dimensions with high coefficients of determination (R^2). Additionally, Fig. 7 shows the linear correlation between the porosity of the SLM Ti6Al4V structures and the model CAD porosity, showing a determination coefficient of 97.8%.

Considering that these deviations are systematically found for Ti6Al4V structures produced by SLM, the linear correlations shown in Figs. 6 and 7 allow to predict and estimate the real dimensions of Ti6Al4V cellular structures. This data can be used as design guidelines to help engineers fabricating near-net shape SLM Ti6Al4V cellular structures [48,49].

The average dimensions of the open-cell and walls were used to construct adjusted CAD models aiming to obtain numerical models with dimensions and mechanical responses matching to the SLM produced. The porosity obtained experimentally and the porosity of the Model CADs, and the Adjusted CADs was compared then compared as shown in Fig. 8.

The methodology adopted for modelling the adjusted CAD allowed to obtain structures with a porosity similar to the ones measured in SLM structures, as shown in Fig. 8. It can be observed that the SLM structures lower open-cell sizes and the thicker walls (Fig. 5) led to an expected lower porosity. On average, a 30% lower porosity was found when comparing the SLM structures with the model CAD and a 2% higher porosity when comparing with the adjusted CAD.

3.2. Mechanical characterization

Bone tissue is a self-optimizing structure able to adapt to external loading conditions. According to Frost's mechanostat theory, the biological response of bone depends on the level of strain that is induced [50,51]. The stiffness mismatch between bone and currently used hip implant solutions leads to an inefficient stress distribution, that induce stress shielding and finally can lead to implant failure [27,28]. Typically, 10–20 years after Total Hip arthroplasty, revision surgeries are necessary and this mismatch is pointed out as one of the main reasons [23]. Therefore, in the present study, Ti6Al4V structures different porosity levels were designed, SLM produced and characterized targeting the development of new orthopedic implant solutions capable to reduce revision surgeries.

Fig. 9 shows typical experimental load-displacement curves (P-δ curves) obtained for each Ti6Al4V cellular structure, in the linear elastic regime (with corresponding linear correlations).

Finite elements analyses were carried out using the model CADs and the adjusted CADs. Fig. 10 shows the stress fields (von Mises) obtained for SP1 (Model CAD) and SP5 (Adjusted CAD) for a given displacement increment within the material elastic domain (tested experimentally).

The analysis of Fig. 10 allows identifying a symmetric (von Mises) stress field, with higher values in the mid-span. A homogenous stress distribution is also visible throughout the model. The P-δ curves obtained both numerically and experimentally were then used to estimate the exact value of the elastic modulus (E) by means of Equation (1). This procedure was adopted considering the influence of the loading-span (L) on the attained value of E. Effectively, the exact value of E results from a sufficiently high value of L, which allows respecting the Bernoulli-Euler beam theory. Fig. 11 shows the average elastic modulus obtained for the numerical results (model CAD and adjusted CAD) and also for the experimental results. The elastic modulus of cortical bone tissue is also included in Fig. 11 for comparison purposes, according reference [22]. The elastic modulus differences between the SP1, SP2, SP3, SP4 and SP5 are statistically significant.

Analyzing Fig. 11, several aspects can be pointed. As expected, considering the porosity measurements (Fig. 8) the elastic modulus obtained in the numerical study for the model CAD were lower for all

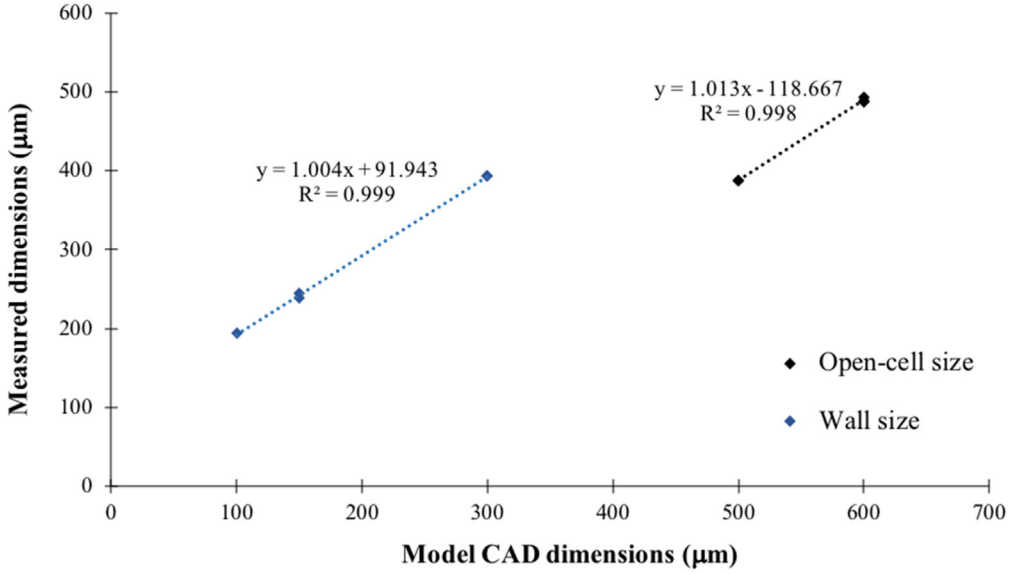

Fig. 6. Correlations between the measured dimensions and the Model CAD dimensions.

the studied structures, comparatively to the ones obtained experimentally. It can also be observed that similar values of elastic modulus were obtained when comparing the numerical results (adjusted CAD) with the experimental ones. The adjusted CAD models allowed to reproduce numerically the mechanical response obtained experimentally. Therefore, FE analysis proved to be an effective tool to simulate the mechanical response of SLM structures.

Ti6Al4V structure with the lowest porosity (45%) exhibited the higher elastic modulus, i.e., 39 GPa. On the other hand, the Ti6Al4V structure with the highest value of porosity exhibited the lowest value of elastic modulus, i.e., 11 GPa. It was found that SP3 Ti6Al4V cellular structure with an open-cell and wall sizes of 388 µm and 244 µm, respectively, and a resulting porosity of ≈ 65%, exhibited a flexural elastic modulus of 21 GPa. Consequently, the SP3 and SP4 geometries can be viewed as the most adequate solutions to be applied in the production of Ti6Al4V orthopedic implants, since they attained the target value of elastic modulus characteristic of cortical bone tissue.

3.3. Surface roughness, wettability and capillarity tests

The interaction between the implant and cortical bone tissue depends on the combination of several aspects [7,54]. In this sense, besides the elastic modulus, other properties were inspected in this study, namely the surface roughness, wettability and capillarity. In fact, surface properties and capillarity play a crucial role in the implant integration with the bone tissue [35,55,56]. An efficient implant-bone biological interaction is influenced by the adhesion and spreading ability of cells on implant surfaces. Several surface properties (e.g., roughness, wettability, chemical composition and morphology) are pointed as affecting the cellular responses when in contact with biomaterials, and can be used to enhance implant integration [31,33,57].

Fig. 12 shows SEM images of the as-produced, polished and sand-blasted surfaces of SP3 and SP5 structures. Table 5 shows the average surface roughness (R_a) values obtained for SP1, SP2, SP3, SP4 and SP5 specimens.

Implants with suitable roughness have been proven to enhance the differentiation of bone-forming cells (osteoblasts), to reduce the activity

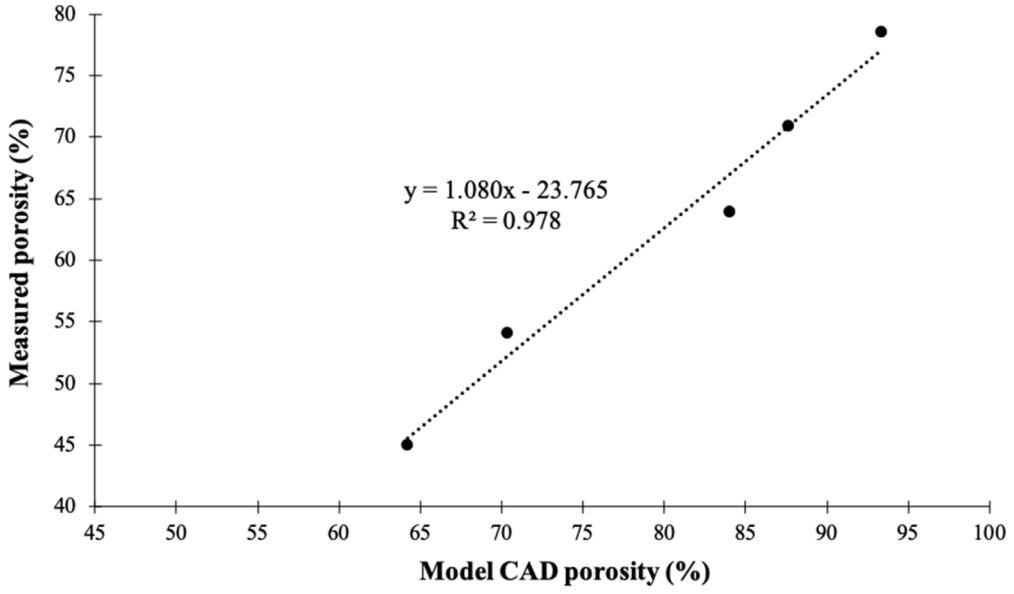

Fig. 7. Correlation between the measured porosity and the CAD design porosity.

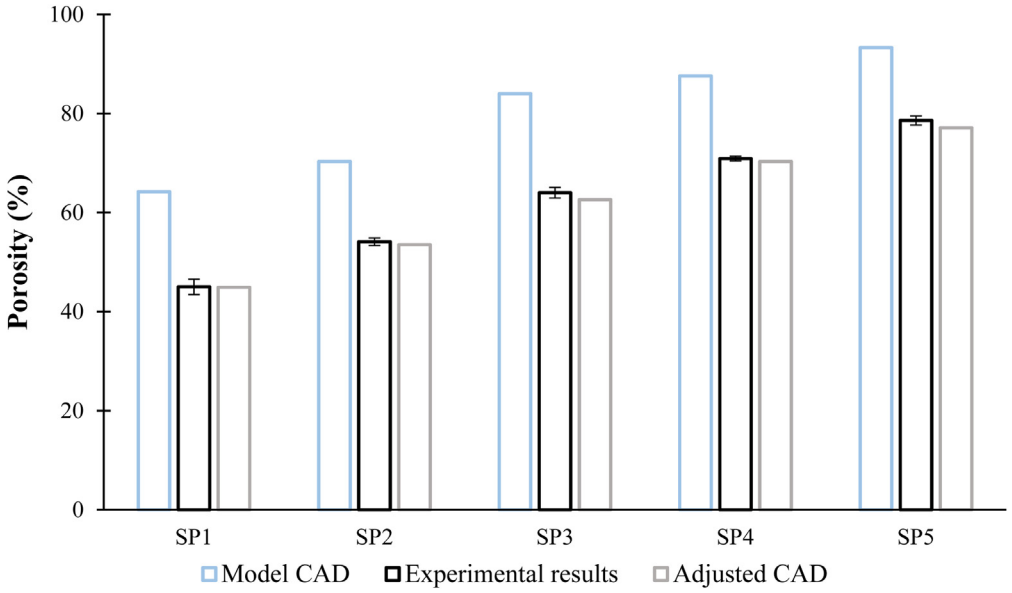

Fig. 8. Experimental and numerical porosities.

of bone-resorption cells (osteoclasts) and to promote bone attachment to the implant surface and its mineralization [28–31]. When regarding the as-produced structures, a surface roughness around 13 μm was found, which is in consistency with several reported studies that used a similar powder distribution to produce Ti6Al4V SLM components [12,35]. As reported in Table 5, the sandblasted surface treatment allowed to obtain a surface roughness (R_a) between 2.2 and 2.9 μm. These results are within the range of values reported for the enhancement of implant osteointegration. Several implant systems, such as Straumann, Bego and Ankylos [58] use surface preparations to obtain a microroughness between 2 and 4 μm (R_a) [52,59,60]. In fact, several clinical and in vivo studies [28,29] have demonstrated that moderate surface roughness lead to earlier healing, enhanced cell spreading, tissue integration and bone formation. For each condition (as-produced, polished and sandblasted) no significant differences were found between the specimens (SP1 to SP5) indicating the homogeneity of each condition/treatment. On the other hand, when comparing the different treatments for the same structure type, all the results have significative differences indicating that each surface condition/treatment induces specific surface roughness different from the others.

When regarding the wettability tests, for all the as-produced surfaces, contact angles higher than 90º were obtained, indicating a hydrophobic behavior. The contact angles obtained were 154.56° ± 8.5, 169.94° ± 17.3, 164.32° ± 17.6, 144.40° ± 10.3 and 161.36° ± 23.1 for SP1, SP2, SP3, SP4 and SP5, respectively. These results show that these SLM as-produced surfaces naturally repel the PBS liquid causing the droplets to form. Fig. 13 shows a typical hydrophobic behavior observed for SP4 specimen, as an example.

Contrarily to the as-produced surfaces, for the polished and sandblasted surfaces it was not possible to measure the contact angle. In those cases, it was noticed that in three consecutive frames the drop spreading is complete (Fig. 14). The polishing and sandblasting surface treatments led to a higher liquid affinity resulting in a spread across maximizing the contact. Besides the surface morphology (roughness

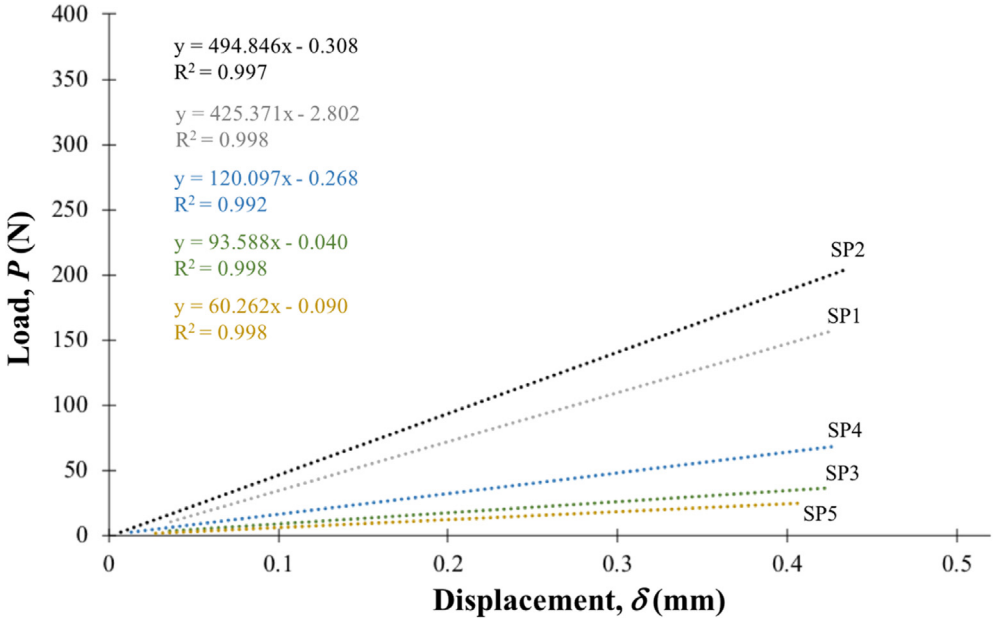

Fig. 9. Experimental P-δ curves with linear fit for SP1, SP2, SP3, SP4 and SP5 Ti6Al4V structures.

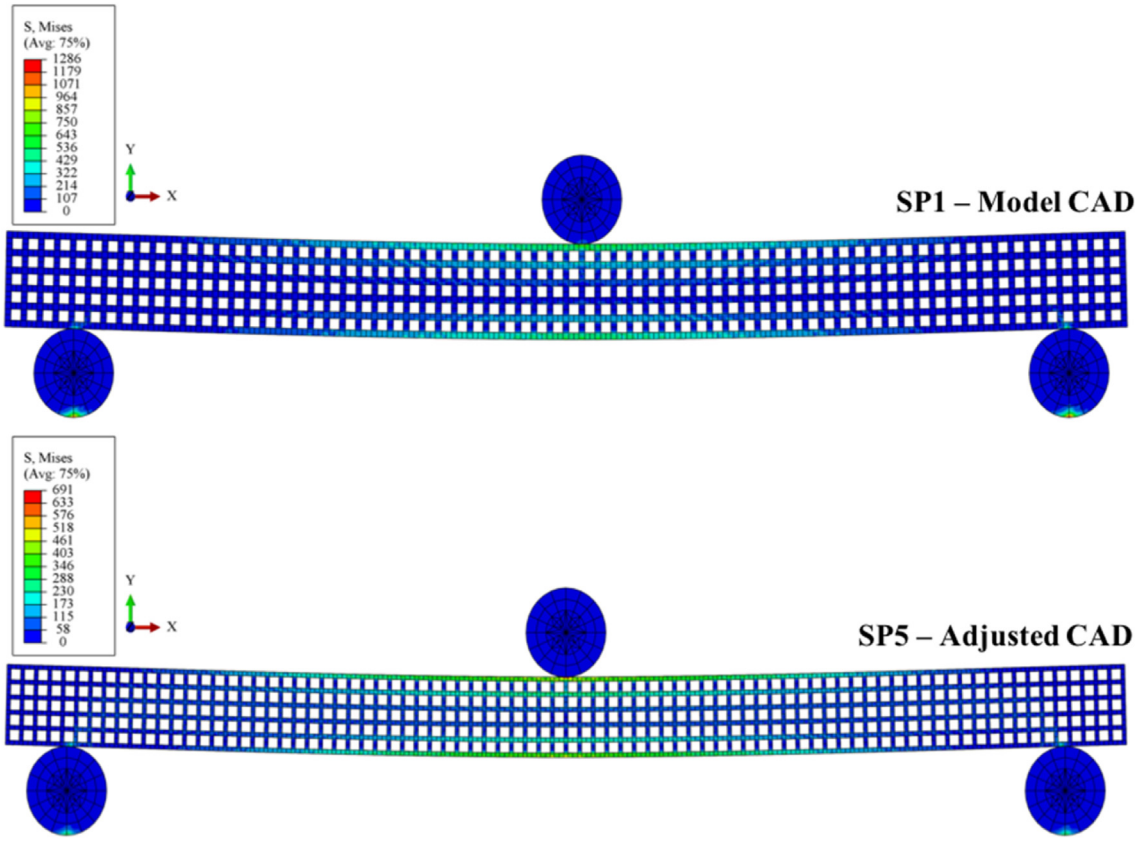

Fig. 10. Stress field (von Mises) of the SP1 (Model CAD) and SP5 (Adjusted CAD CAD).

profile) of the specimen walls, the existence of open-cells plays an important role on the surface wettability [35]. The air present inside the cellular structures affects the structure wettability. In fact, the effect of the air pockets is only disrupted when the capillarity forces exceed this pressure [61].

While all the as-produced specimens showed a hydrophobic behavior, the same specimens when polished or sandblasted became super hydrophilic (supplementary videos 1 and 2 – SP1 polished and SP5 sandblasted structures, respectively). It remains unclear which is the suitable hydrophilicity range to promote the best biological interaction on implants surface. However, it is known that there is a direct correlation between the wettability and cell adhesion (higher wettability leads to enhanced adhesion). Several studies indicate that hydrophilic surfaces are usually preferred rather than hydrophobic since they promote an enhanced implant-bone interaction [32,35]. As an example, Zhao et al. [33] concluded that osteoblast-cells cultured hydrophilic

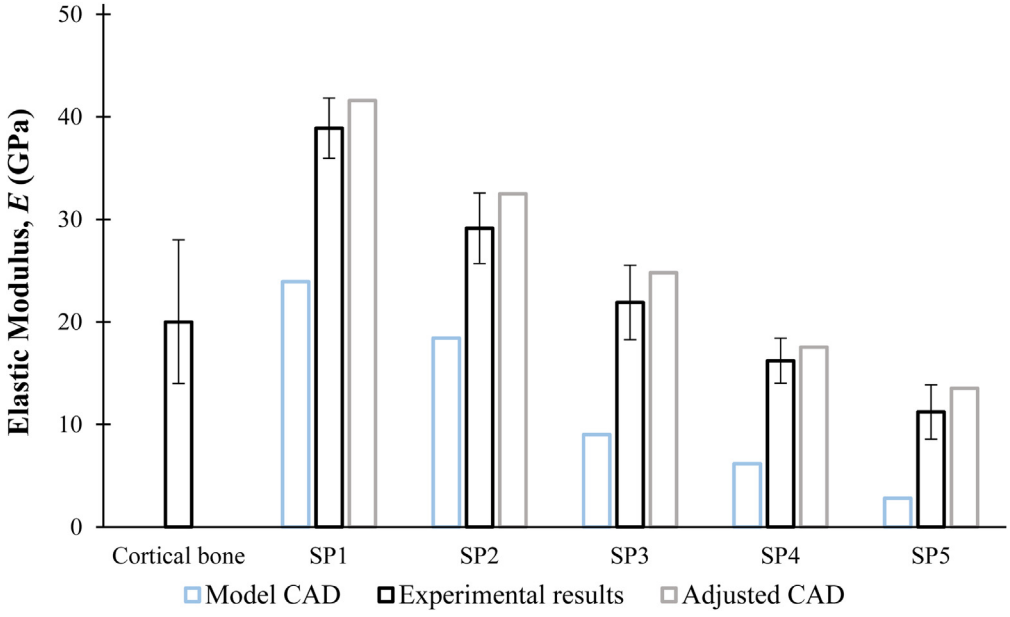

Fig. 11. Experimental and numerical elastic modulus of SP1, SP2, SP3, SP4 and cortical bone.

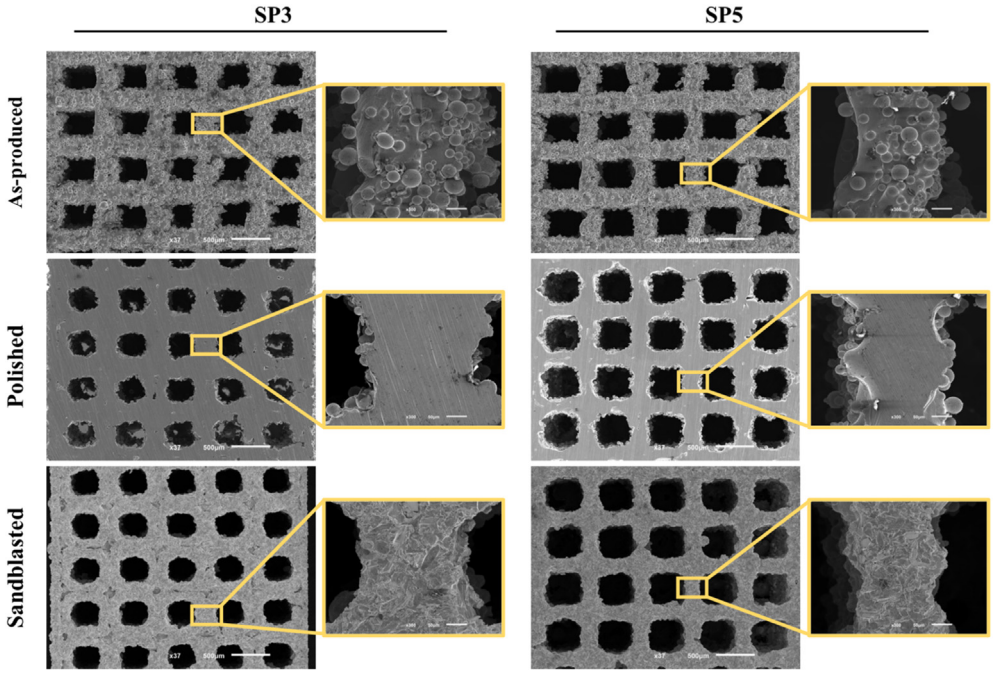

Fig. 12. SEM images of the as-produced, polished and sandblasted surfaces for SP3 and SP5 structures.

Table 5
Average surface roughness (R_a) measurements for SP1, SP2, SP3, SP4 and SP5 Ti6Al4V structures.

	As-produced (μm)	Polished (μm)	Sandblasted (μm)
SP1	12.64 ± 2.66	1.98 ± 0.74	2.77 ± 0.20
SP2	11.61 ± 1.33	1.77 ± 1.09	2.21 ± 0.46
SP3	12.86 ± 2.58	1.82 ± 0.96	2.89 ± 0.72
SP4	13.01 ± 1.37	1.84 ± 1.09	2.50 ± 0.72
SP5	14.07 ± 3.53	1.45 ± 0.21	2.62 ± 0.34

surfaces produced more differentiation markers represented by increased cell layer alkaline phosphatase specific activity.

Supplementary video related to this article can be found at https://doi.org/10.1016/j.msec.2019.110342.

The capillarity ability is another relevant property when designing orthopedic implants [56]. In fact, the capillary action is used in nature to transport water and nutrients based on morphological and/or chemical gradient structures [38]. For instance, in the circulatory system, blood movement proceeds in microscopic capillaries from arterioles to venules by capillary action [37]. Fig. 15 shows images (frames corresponding to different time points) obtained during the capillarity tests and also the fluid height measured on 0.25 s, 0.5 s, 1.0 s and 2.0 s after the specimen touches the fluid.

Fig. 15 shows that PBS had the ability to flow in the Ti6Al4V structures without any assistance and in opposition to gravity. This capillarity action was observed for all the structures and were observed fluid heights of 20.03, 13.54, 12.64, 11.25 and 9.36 mm for SP1, SP2, SP3, SP4 and SP5, respectively (supplementary video 3 – SP1 structure). Polak et al. [39] and Bai et al. [38] demonstrated that capillary forces play an important role in cells self-seeding and cell attachment on scaffolds surfaces.

Supplementary video related to this article can be found at https://doi.org/10.1016/j.msec.2019.110342.

Despite the hydrophobic behavior seen for the as-produced surfaces (Fig. 16) these results prove that as-produced Ti6Al4V cellular structures are able to transport PBS fluid along its structure. SP1 structure exhibited the highest fluid height, of 20.03 mm reached after 2.0 s, being unaltered for the ensuing time. This highest fluid height was observed for the Ti6Al4V structure with the lowest porosity (45.0% -

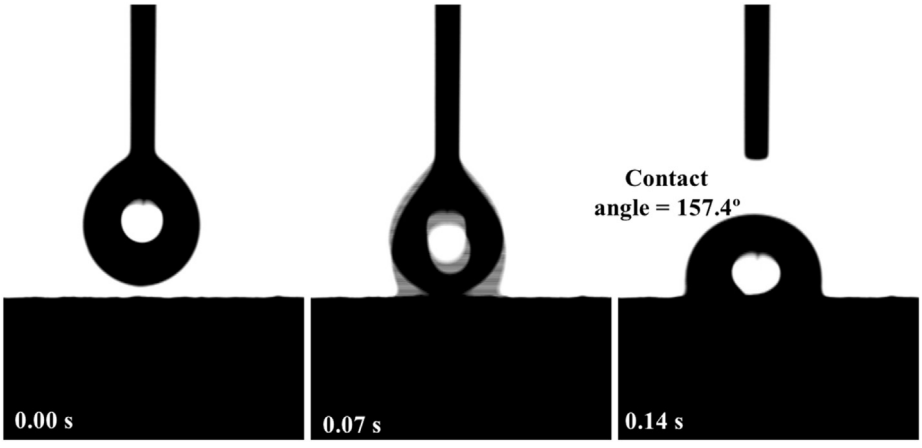

Fig. 13. Hydrophobic behavior of SP4 as-produced surface.

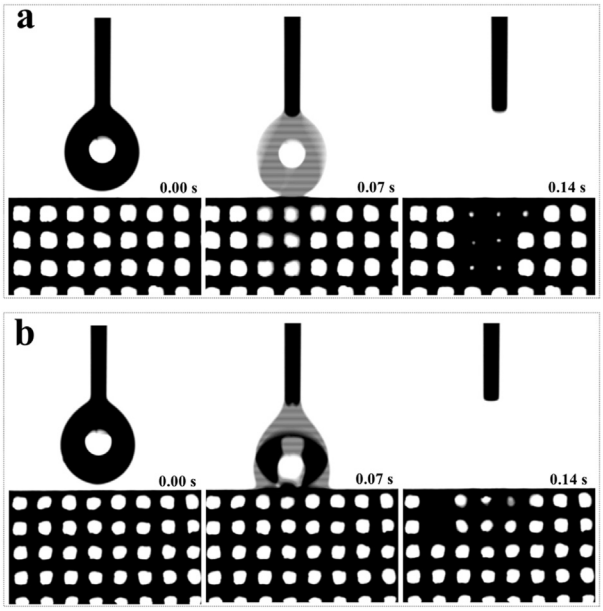

Fig. 14. Typical super hydrophilic behavior found for (a) SP5 polished surface and (b) SP3 sandblasted surface.

SP1). Contrarily, the lowest fluid heights were observed for SP5 and SP4, corresponding to the specimens with the highest porosity, 70.9 and 78.6%, respectively. These results indicate that the capillarity pressure is higher for structures with a lower porosity (lower hollow volume) leading to a higher fluid height [62]. In fact, when comparing SP1 and SP3 (structures with an open-cell size around 400 μm) it is possible to understand that as higher wall size, as lower the porosity, which leads to a higher the fluid height.

3.4. Cell viability

The cytotoxicity of the produced specimens was assessed in order to ascertain the toxic effect of the products released from the metallic structures during incubation with MEM. Cell viability of L929 cells after culturing for 24 h, 7, 14, 21 and 28 days was assessed and the overall results are present in Fig. 16.

Fig. 16 shows the viability results of the Ti6Al4V cellular structures produced by SLM, for five different timepoints. The statistical analysis performed allow to understand that no significant differences were observed for all the timepoints of MEM extraction compared to the positive control. Considering these results, it can be assumed that the Ti6Al4V cellular structures SLM produced did not release toxic substances to the medium, indicating that these structures can assure a suitable environment for cells to proliferate and attach [35].

3.5. Hip implant prototype

In this study, a multi-functional design for hip implants considering Ti6Al4V cellular structures with a suitable combination of mechanical properties, porosity, roughness, wettability, capillarity and cell viability is proposed. A prototype was fabricated to assess the technical capacity to produce a Ti6Al4V hip implant using a SLM commercial equipment

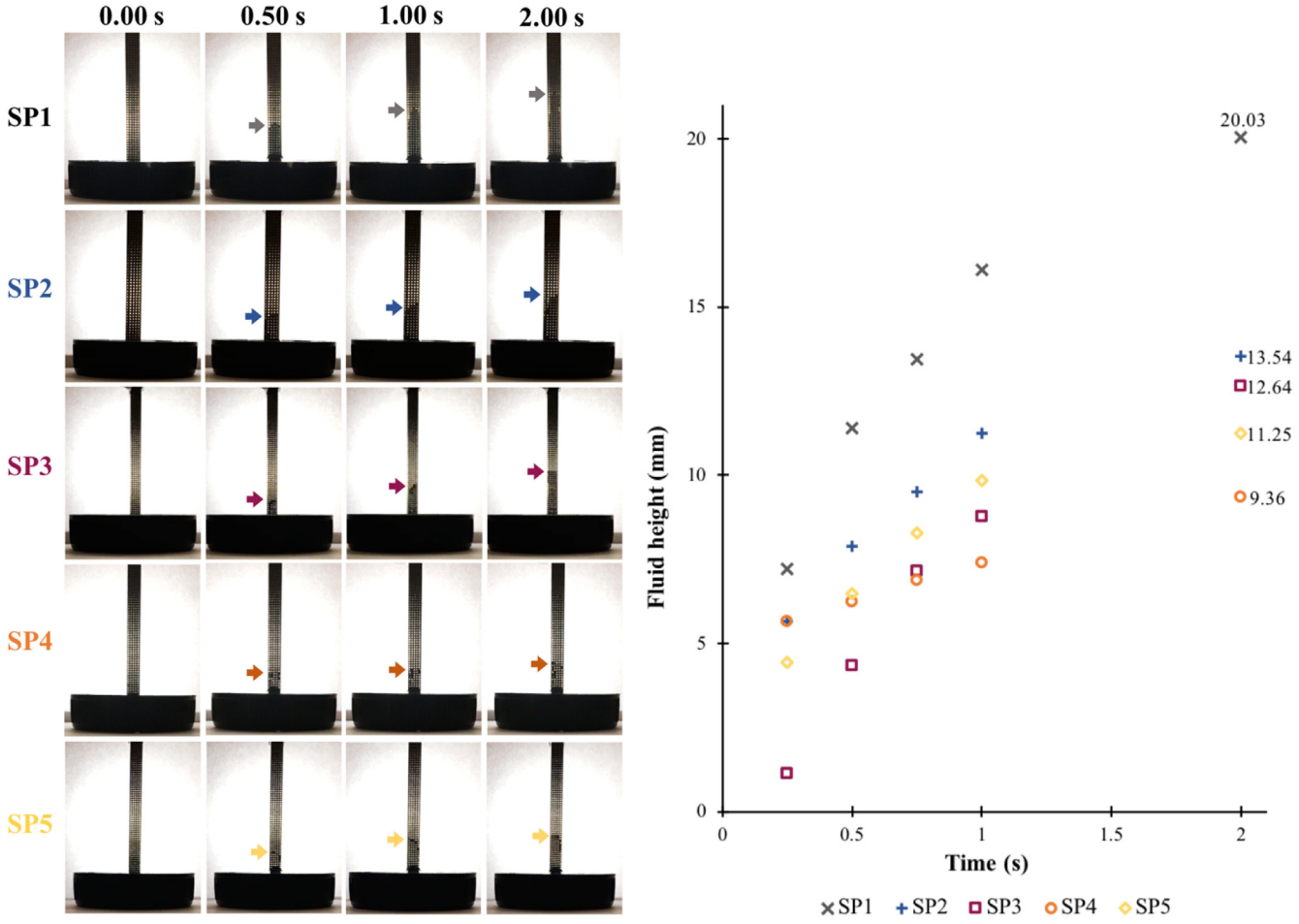

Fig. 15. Capillary tests timeframes and corresponding fluid height results.

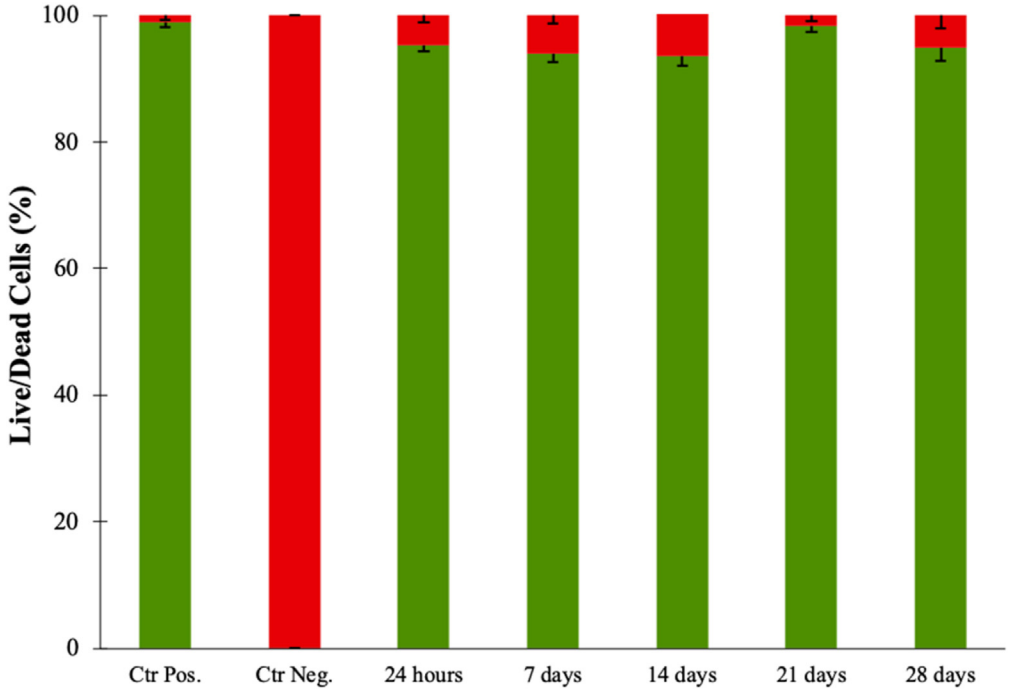

Fig. 16. Cell viability of L929 cells after culturing for 24 h, 7, 14, 21 and 28 days.

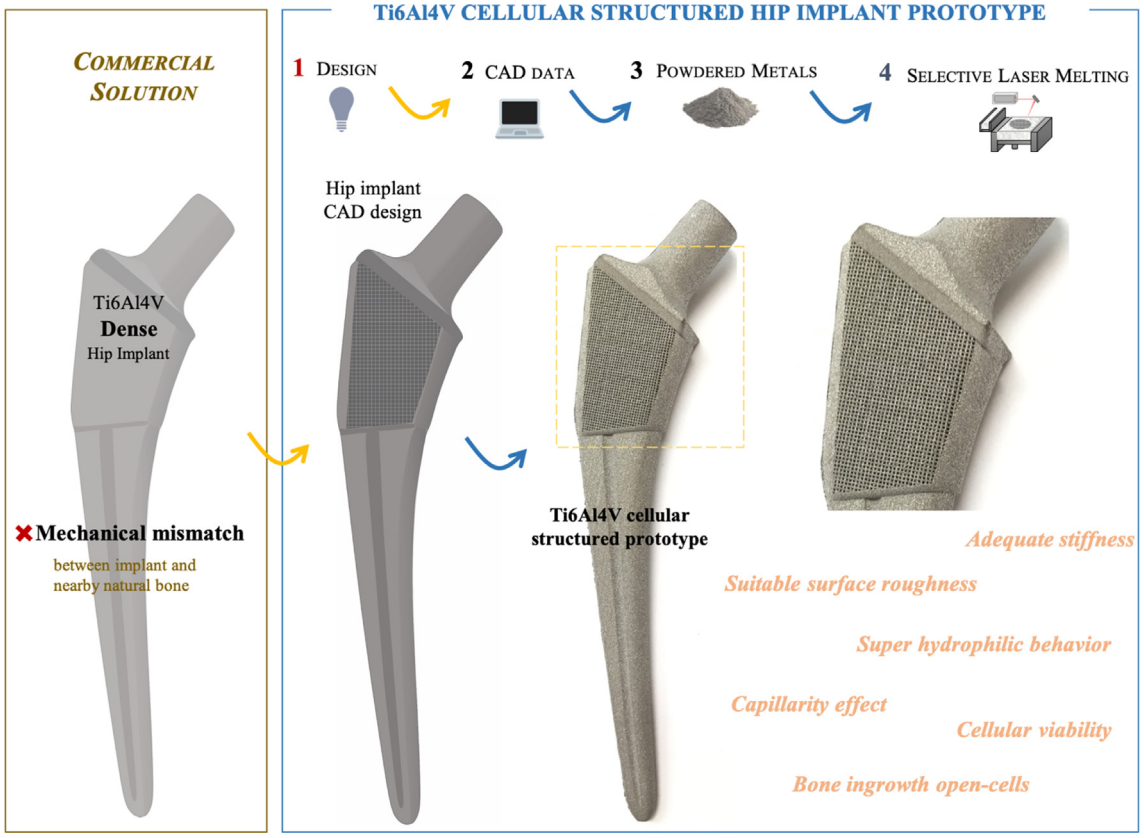

Fig. 17. Ti6Al4V cellular structured hip implant prototype.

(see section 2.1). This hip implant prototype was modeled by re-engineering a commercial hip implant. The obtained CAD was then modified to create a full cellular structured hip implant. After optimizing the SLM fabrication parameters that includes the supports preparation/definition (type, orientation and distribution) and the implant positioning, a Ti6Al4V cellular structured hip implant was successfully produced as shown in Fig. 17.

This prototype has an open transversal cellular structure region opened from side to side. Excluding the above-mentioned region, the remaining implant is internally cellular structured with a dense outer shell of 300 μm thick. The cellular structure was defined considering the suitable elastic modulus of SP3 structure (≈ 20 GPa), as seen in Fig. 11.

This architecture (SP3 structure) displays an open-cell size of ≈ 400 μm and a wall size of ≈ 250 μm, resulting in a porosity of ≈ 64%. Additionally, this implant can also display a suitable combination of surface roughness, wettability and capillarity, found adequate to promote an improved implant stability. This prototype or miniaturized versions are being considered for ensuing in vivo experiments.

4. Conclusions

- A set of fundamental tools is provided to improve the design and the production of Ti6Al4V structures by Selective Laser Melting technique;
- Linear correlations were systematically found between the dimension/porosity of the SLM structures and the designed model CAD dimensions/porosity;
- Finite element models (Adjusted CADs) were constructed using the dimensions obtained experimentally to reproduce the mechanical response of the SLM structures;
- The obtained data can be used in FE analysis as design guidelines to help engineers fabricating near-net shape SLM Ti6Al4V cellular structures;
- The cell viability analyses show that the SLM produced structures did not release toxic substances to the medium;
- Besides suitable mechanical properties and a design methodology, this study proposes an accurate combination of porosity, roughness, wettability and capillarity, all of them relevant for the production of novel orthopedic implant solutions;
- A Ti6Al4V cellular structured hip implant prototype gathering the suitable features addressed in this study was successfully SLM-produced.

Declaration of competing interest

The authors have no conflicts of interest to declare.

Acknowledgements

This work was supported by FCT through the grants SFRH/BD/128657/2017 and SFRH/BPD/112111/2015, the projects PTDC/EMS-TEC/5422/2014 (ADAPTPROSTHESIS) and POCI-01-0145-FEDER-030353 (SMARTCUT) and also by project NORTE 01–0145_FEDER-000018. Additionally, this work was supported by FCT with the reference project UID/EEA/04436/2019, by FEDER funds through the COMPETE 2020 – Programa Operacional Competitividade e Internacionalização (POCI) with the reference project POCI-01-0145-FEDER-006941.

References

[1] L. Zhang, S. Zhang, H. Zhu, Z. Hu, G. Wang, X. Zeng, Horizontal dimensional accuracy prediction of selective laser melting, Mater. Des. 160 (2018) 9–20, https://doi.org/10.1016/J.MATDES.2018.08.059.

[2] H. Zhang, H. Zhu, T. Qi, Z. Hu, X. Zeng, Selective laser melting of high strength Al-Cu-Mg alloys: processing, microstructure and mechanical properties, Mater. Sci. Eng. A 656 (2016) 47–54, https://doi.org/10.1016/j.msea.2015.12.101.

[3] M. Speirs, B. Van Hooreweder, J. Van Humbeeck, J.P. Kruth, Fatigue behaviour of NiTi shape memory alloy scaffolds produced by SLM, a unit cell design comparison, J. Mech. Behav. Biomed. Mater. 70 (2017) 53–59, https://doi.org/10.1016/j.jmbbm.2017.01.016.

[4] X. Wang, S. Xu, S. Zhou, W. Xu, M. Leary, P. Choong, M. Qian, M. Brandt, Y.M. Xie, Topological design and additive manufacturing of porous metals for bone scaffolds and orthopaedic implants: a review, Biomaterials 83 (2016) 127–141, https://doi.org/10.1016/j.biomaterials.2016.01.012.

[5] B. Van Hooreweder, Y. Apers, K. Lietaert, J.P. Kruth, Improving the fatigue performance of porous metallic biomaterials produced by Selective Laser Melting, Acta Biomater. 47 (2017) 193–202, https://doi.org/10.1016/j.actbio.2016.10.005.

[6] F. Bartolomeu, M. Buciumeanu, E. Pinto, N. Alves, F.S. Silva, O. Carvalho, G. Miranda, Wear behavior of Ti6Al4V biomedical alloys processed by selective laser melting, hot pressing and conventional casting, Trans. Nonferrous Met. Soc. China (English Ed). 27 (2017) 829–838, https://doi.org/10.1016/S1003-6326(17)60060-8.

[7] F.S.L. Bobbert, K. Lietaert, A.A. Eftekhari, B. Pouran, S.M. Ahmadi, H. Weinans, A.A. Zadpoor, Acta Biomaterialia Additively manufactured metallic porous biomaterials based on minimal surfaces : a unique combination of topological , mechanical , and mass transport properties, Acta Biomater. 53 (2017) 572–584, https://doi.org/10.1016/j.actbio.2017.02.024.

[8] F. Bartolomeu, M. Buciumeanu, M.M. Costa, N. Alves, M. Gasik, F.S. Silva, G. Miranda, Multi-material Ti6Al4V & PEEK cellular structures produced by Selective Laser Melting and Hot Pressing : a tribocorrosion study targeting orthopedic applications, J. Mech. Behav. Biomed. Mater. 89 (2019) 54–64, https://doi.org/10.1016/j.jmbbm.2018.09.009.

[9] G. Ryan, A. Pandit, D.P. Apatsidis, Fabrication methods of porous metals for use in orthopaedic applications, Biomaterials 27 (2006) 2651–2670, https://doi.org/10.1016/j.biomaterials.2005.12.002.

[10] M. Buciumeanu, S. Almeida, F. Bartolomeu, M.M. Costa, N. Alves, F.S. Silva, G. Miranda, Ti6Al4V cellular structures impregnated with biomedical PEEK - new material design for improved tribological behavior, Tribol. Int. 119 (2018) 157–164, https://doi.org/10.1016/j.triboint.2017.10.038.

[11] Z.S. Bagheri, D. Melancon, L. Liu, R.B. Johnston, D. Pasini, Compensation strategy to reduce geometry and mechanics mismatches in porous biomaterials built with Selective Laser Melting, J. Mech. Behav. Biomed. Mater. 70 (2017) 17–27, https://doi.org/10.1016/j.jmbbm.2016.04.041.

[12] F. Bartolomeu, M. Sampaio, O. Carvalho, E. Pinto, N. Alves, J.R. Gomes, F.S. Silva, G. Miranda, Tribological behavior of Ti6Al4V cellular structures produced by Selective Laser Melting, J. Mech. Behav. Biomed. Mater. 69 (2017) 128–134, https://doi.org/10.1016/j.jmbbm.2017.01.004.

[13] S. Arabnejad, R.B. Johnston, J. Ann, B. Singh, M. Tanzer, D. Pasini, High-strength porous biomaterials for bone replacement : a strategy to assess the interplay between cell morphology , mechanical properties , bone ingrowth and manufacturing constraints, Acta Biomater. 30 (2016) 345–356, https://doi.org/10.1016/j.actbio.2015.10.048.

[14] J. Kadkhodapour, H. Montazerian, A.C. Darabi, A.P. Anaraki, Failure mechanisms of additively manufactured porous biomaterials : effects of porosity and type of unit cell, J. Mech. Behav. Biomed. Mater. 50 (2015) 180–191, https://doi.org/10.1016/j.jmbbm.2015.06.012.

[15] M. Smith, Z. Guan, W.J. Cantwell, Finite element modelling of the compressive response of lattice structures manufactured using the selective laser melting technique, Int. J. Mech. Sci. 67 (2013) 28–41, https://doi.org/10.1016/j.ijmecsci.2012.12.004.

[16] C.G. Moura, R. Pereira, M. Buciumeanu, O. Carvalho, F. Bartolomeu, R. Nascimento, F.S. Silva, Effect of laser surface texturing on primary stability and surface properties of zirconia implants, Ceram. Int. 43 (2017) 15227–15236, https://doi.org/10.1016/j.ceramint.2017.08.058.

[17] Q. Chen, G.A. Thouas, Metallic implant biomaterials, Mater. Sci. Eng. R Rep. 87 (2015) 1–57, https://doi.org/10.1016/j.mser.2014.10.001.

[18] M. Dallago, V. Fontanari, E. Torresani, M. Leoni, C. Pederzolli, C. Potrich, M. Benedetti, Fatigue and biological properties of Ti-6Al-4V ELI cellular structures with variously arranged cubic cells made by selective laser melting, J. Mech. Behav. Biomed. Mater. 78 (2018) 381–394, https://doi.org/10.1016/j.jmbbm.2017.11.044.

[19] S.Y. Chen, J.C. Huang, C.T. Pan, C.H. Lin, T.L. Yang, Y.S. Huang, C.H. Ou, L.Y. Chen, D.Y. Lin, H.K. Lin, T.H. Li, J.S.C. Jang, C.C. Yang, Microstructure and Mechanical Properties of Open-Cell Porous Ti-6Al- 4V Fabricated by Selective Laser Melting vol.713, (2017), pp. 248–254, https://doi.org/10.1016/j.jallcom.2017.04.190.

[20] M. Fousová, D. Vojt, E. Jablonská, J. Fojt, Characteristics of gradient porosity Ti-6Al-4V alloy prepared by SLM process, J. Mech. Behav. Biomed. Mater. Promising. 69 (2017) 368–376, https://doi.org/10.1016/j.jmbbm.2017.01.043.

[21] S. Bose, D. Ke, H. Sahasrabudhe, A. Bandyopadhyay, Progress in materials science additive manufacturing of biomaterials, Prog. Mater. Sci. 93 (2018) 45–111, https://doi.org/10.1016/j.pmatsci.2017.08.003.

[22] J. Capek, M. Machová, M. Fousová, J. Kubbásek, D. Vojtechch, J. Fojt, E. Jablonská, J. Lipov, T. Ruml, Highly porous, low elastic modulus 316L stainless steel scaffold prepared by selective laser melting, Mater. Sci. Eng. C 69 (2016) 631–639, https://doi.org/10.1016/j.msec.2016.07.027.

[23] U. Holzwarth, G. Cotogno, Total Hip Arthroplasty (2012), https://doi.org/10.2788/31286.

[24] F. Bartolomeu, C.S. Abreu, C.G. Moura, M.M. Costa, N. Alves, F.S. Silva, G. Miranda, Ti6Al4V-PEEK multi-material structures – design, fabrication and tribological characterization focused on orthopedic implants, Tribol. Int. 131 (2018) 672–678, https://doi.org/10.1016/j.triboint.2018.11.017.

[25] M.M. Costa, R. Lima, F. Melo-Fonseca, F. Bartolomeu, N. Alves, A. Miranda, M. Gasik, F.S. Silva, N.A. Silva, G. Miranda, Development of β -TCP-Ti6Al4V structures : driving cellular response by modulating physical and chemical properties, Mater. Sci. Eng. C 98 (2019) 705–716, https://doi.org/10.1016/j.msec.2019.01.016.

[26] B. Thavornyutikarn, N. Chantarapanich, Q. Chen, Bone Tissue Engineering Scaffolding : Computer-Aided Scaffolding Techniques, (2014), https://doi.org/10.1007/s40204-014-0026-7.

[27] F. Bartolomeu, J. Fonseca, N. Peixinho, N. Alves, M. Gasik, F.S. Silva, G. Miranda, Predicting the output dimensions , porosity and elastic modulus of additive manufactured biomaterial structures targeting orthopedic implants, J. Mech. Behav. Biomed. Mater. 99 (2019) 104–117, https://doi.org/10.1016/j.jmbbm.2019.07.023.

[28] M. de Wild, R. Schumacher, K. Mayer, E. Schkommodau, D. Thoma, M. Bredell, A. Kruse Gujer, K.W. Grätz, F.E. Weber, Bone regeneration by the osteoconductivity of porous titanium implants manufactured by selective laser melting: a histological

and micro computed tomography study in the rabbit, Tissue Eng. A 19 (2013) 2645–2654, https://doi.org/10.1089/ten.TEA.2012.0753.
[29] Straumann, Scientific Evidence First Edition, (2011), pp. 1–36.
[30] Z. Schwartz, P. Raz, G. Zhao, Y. Barak, M. Tauber, H. Yao, B.D. Boyan, Effect of micrometer-scale roughness of the surface of Ti6Al4V pedicle screws in vitro and in vivo, J. Bone Joint Surg. Am. 90 (2008) 2485–2498, https://doi.org/10.2106/JBJS.G.00499.
[31] G. Zhao, A.L. Raines, M. Wieland, Z. Schwartz, B.D. Boyan, Requirement for both micron- and submicron scale structure for synergistic responses of osteoblasts to substrate surface energy and topography, Biomaterials 28 (2007) 2821–2829, https://doi.org/10.1016/j.biomaterials.2007.02.024.
[32] R.A. Gittens, L. Scheideler, F. Rupp, S.L. Hyzy, J. Geis-Gerstorfer, Z. Schwartz, B.D. Boyan, A review on the wettability of dental implant surfaces II: biological and clinical aspects, Acta Biomater. 10 (2014) 2907–2918, https://doi.org/10.1016/j.actbio.2014.03.032.
[33] G. Zhao, Z. Schwartz, M. Wieland, F. Rupp, J. Geis-Gerstorfer, D.L. Cochran, B.D. Boyan, High surface energy enhances cell response to titanium substrate microstructure, J. Biomed. Mater. Res. A 74 (2005) 49–58, https://doi.org/10.1002/jbm.a.30320.
[34] L. Le Guéhennec, A. Soueidan, P. Layrolle, Y. Amouriq, Surface treatments of titanium dental implants for rapid osseointegration, Dent. Mater. 23 (2007) 844–854, https://doi.org/10.1016/j.dental.2006.06.025.
[35] F. Melo-Fonseca, R. Lima, M.M. Costa, F. Bartolomeu, N. Alves, A. Miranda, M. Gasik, F.S. Silva, N.A. Silva, G. Miranda, 45S5 BAG-Ti6Al4V structures: the influence of the design on some of the physical and chemical interactions that drive cellular response, Mater. Des. 160 (2018) 95–105, https://doi.org/10.1016/j.matdes.2018.08.056.
[36] D. Buser, N. Broggini, M. Wieland, R.K. Schenk, A.J. Denzer, D.L. Cochran, B. Hoffmann, A. Lussi, S.G. Steinemann, J. Dent. Res. (2004), https://doi.org/10.1177/154405910408300704.
[37] D.S. Oh, Y.J. Kim, M.H. Hong, M.H. Han, K. Kim, Effect of capillary action on bone regeneration in micro-channeled ceramic scaffolds, Ceram. Int. 40 (2014) 9583–9589, https://doi.org/10.1016/j.ceramint.2014.02.033.
[38] H. Bai, D. Wang, B. Delattre, W. Gao, J. De Coninck, S. Li, A.P. Tomsia, Biomimetic gradient scaffold from ice-templating for self-seeding of cells with capillary effect, Acta Biomater. 20 (2015) 113–119, https://doi.org/10.1016/j.actbio.2015.04.007.
[39] S.J. Polak, L.E. Rustom, G.M. Genin, M. Talcott, A.J.W. Johnson, HHS Public Access 9 (2019) 7977–7986, https://doi.org/10.1016/j.actbio.2013.04.040.A.
[40] F. Bartolomeu, S. Faria, O. Carvalho, E. Pinto, N. Alves, F.S. Silva, G. Miranda, Predictive models for physical and mechanical properties of Ti6Al4V produced by Selective Laser Melting, Mater. Sci. Eng. A 663 (2016) 181–192, https://doi.org/10.1016/j.msea.2016.03.113.
[41] V. Karageorgiou, D. Kaplan, Porosity of 3D biomaterial scaffolds and osteogenesis, Biomaterials 26 (2005) 5474–5491, https://doi.org/10.1016/j.biomaterials.2005.02.002.
[42] A. Kumar, S. Mandal, S. Barui, R. Vasireddi, U. Gbureck, M. Gelinsky, B. Basu, Low temperature additive manufacturing of three dimensional scaffolds for bone-tissue engineering applications: processing related challenges and property assessment, Mater. Sci. Eng. R Rep. 103 (2016) 1–39, https://doi.org/10.1016/j.mser.2016.01.001.
[43] G. He, P. Liu, Q. Tan, G. Jiang, Flexural and compressive mechanical behaviors of the porous titanium materials with entangled wire structure at different sintering conditions for load-bearing biomedical applications, J. Mech. Behav. Biomed. Mater. 28 (2013) 309–319, https://doi.org/10.1016/j.jmbbm.2013.08.016.
[44] A.J. Salgado, O.P. Coutinho, R.L. Reis, Novel starch-based scaffolds for bone tissue Engineering : Tissue Eng. 10 (2004).
[45] N.A. Silva, B. Sc, A.J. Salgado, D. Ph, R.A. Sousa, D. Ph, J.T. Oliveira, D. Ph, A.J. Pedro, B. Sc, H. Leite-almeida, B. Sc, R. Cerqueira, A. Almeida, D. Ph, Development and Characterization of a Novel Hybrid Tissue Engineering – Based Scaffold for Spinal Cord Injury Repair vol.16, (2010).
[46] Q. Ran, W. Yang, Y. Hu, X. Shen, Y. Yu, Y. Xiang, K. Cai, Osteogenesis of 3D printed porous Ti6Al4V implants with different pore sizes, J. Mech. Behav. Biomed. Mater. 84 (2018) 1–11, https://doi.org/10.1016/j.jmbbm.2018.04.010.
[47] C. Yan, L. Hao, A. Hussein, D. Raymont, International Journal of Machine Tools & Manufacture Evaluations of cellular lattice structures manufactured using selective laser melting, 62 (2012) 32–38, https://doi.org/10.1016/j.ijmachtools.2012.06.002.
[48] N.M. Dhansay, R. Tait, T. Becker, Fatigue and fracture toughness of Ti-6Al-4V titanium alloy manufactured by selective laser melting, Adv. Mater. Res. 1019 (2014) 248–253, https://doi.org/10.4028/www.scientific.net/AMR.1019.248.
[49] M. Fousová, D. Vojtěch, J. Kubásek, E. Jablonská, J. Fojt, Promising characteristics of gradient porosity Ti-6Al-4V alloy prepared by SLM process, J. Mech. Behav. Biomed. Mater. 69 (2017) 368–376, https://doi.org/10.1016/j.jmbbm.2017.01.043.
[50] H.M. Frost, A., Update of bone physiology and Wolff s law for clinicians, Angle Orthod. 74 (2003) 3–15 2004.
[51] M. Piccinini, J. Cugnoni, J. Botsis, P. Ammann, A. Wiskott, Numerical prediction of peri-implant bone adaptation: comparison of mechanical stimuli and sensitivity to modeling parameters, Med. Eng. Phys. 38 (2016) 1348–1359, https://doi.org/10.1016/j.medengphy.2016.08.008.
[52] M. Geetha, A.K. Singh, R. Asokamani, A.K. Gogia, Ti based biomaterials, the ultimate choice for orthopaedic implants - a review, Prog. Mater. Sci. 54 (2009) 397–425, https://doi.org/10.1016/j.pmatsci.2008.06.004.
[54] F. Bartolomeu, M.M. Costa, J.R. Gomes, N. Alves, C.S. Abreu, F.S. Silva, G. Miranda, Implant surface design for improved implant stability – a study on Ti6Al4V dense and cellular structures produced by Selective Laser Melting, Tribol. Int. (2018), https://doi.org/10.1016/j.triboint.2018.08.012.
[55] L. Ponsonnet, K. Reybier, N. Jaffrezic, V. Comte, C. Lagneau, M. Lissac, C. Martelet, Relationship between surface properties (roughness, wettability) of titanium and titanium alloys and cell behaviour, Mater. Sci. Eng. C 23 (2003) 551–560, https://doi.org/10.1016/S0928-4931(03)00033-X.
[56] K. Zhang, Y. Fan, N. Dunne, X. Li, Effect of microporosity on scaffolds for bone tissue engineering, Regen. Biomater. (2018) 115–124, https://doi.org/10.1093/rb/rby001.
[57] C. Yan, L. Hao, A. Hussein, Q. Wei, Y. Shi, Microstructural and surface modifications and hydroxyapatite coating of Ti-6Al-4V triply periodic minimal surface lattices fabricated by selective laser melting, Mater. Sci. Eng. C 75 (2017) 1515–1524, https://doi.org/10.1016/j.msec.2017.03.066.
[58] P. Ming, S. Shao, J. Qiu, J. Yang, Y. Yu, J. Chen, W. Zhu, C. Tang, Superiority of calcium-containing nanowires modified titanium surface compared with SLA titanium surface in biological behavior of osteoblasts: a pilot study, Appl. Surf. Sci. 416 (2017) 790–797, https://doi.org/10.1016/j.apsusc.2017.04.152.
[59] D. Buser, S.F.M. Janner, J.G. Wittneben, U. Brägger, C.A. Ramseier, G.E. Salvi, 10-Year survival and success rates of 511 titanium implants with a sandblasted and acid-etched surface: a retrospective study in 303 partially edentulous patients, Clin. Implant Dent. Relat. Res. 14 (2012) 839–851, https://doi.org/10.1111/j.1708-8208.2012.00456.x.
[60] K. Fischer, T. Stenberg, Prospective 10-year cohort study based on a randomized controlled trial (RCT) on prostheses . Part 1 : sandblasted and acid-etched implants and mucosal tissue, Clin. Implant Dent. Relat. Res. 14 (2012) 1–8, https://doi.org/10.1111/j.1708-8208.2011.00389.x.
[61] S.P. Rodrigues, C.F.A. Alves, A. Cavaleiro, S. Carvalho, Water and oil wettability of anodized 6016 aluminum alloy surface, Appl. Surf. Sci. 422 (2017) 430–442, https://doi.org/10.1016/j.apsusc.2017.05.204.
[62] J. Pinto, A. Athanassiou, D. Fragouli, Effect of the porous structure of polymer foams on the remediation of oil spills, J. Phys. D Appl. Phys. 49 (2016), https://doi.org/10.1088/0022-3727/49/14/145601.